Available online at www.sciencedirect.com
SCIENCE DIRECT®
Journal of Catalysis 220 (2003) 192–206
JOURNAL OF CATALYSIS
www.elsevier.com/locate/jcat

Deactivation pathways in zeolite-catalyzed isobutane/butene alkylation

Andreas Feller, Jan-Olaf Barth, Alexander Guzman, Iker Zuazo, and Johannes A. Lercher *

Lehrstuhl II für Technische Chemie, Technische Universität München, Lichtenbergstr. 4, D-85747 Garching, Germany

Received 25 February 2003; revised 15 May 2003; accepted 28 May 2003

Abstract

The deactivation of rare-earth-exchanged zeolite X as catalysts in isobutane/2-butene alkylation between 40 and 130 °C was studied. The deactivated samples and the isolated deposits were analyzed by a range of techniques, including for the first time (matrix assisted) laser desorption/ionization time-of-flight mass spectroscopy (MALDI-TOF MS, LDI-TOF MS). The compounds found in the deactivated zeolites are, in addition to large alkanes and alkenes, highly unsaturated and highly branched species containing cyclic structures, which are increasingly aromatic as the reaction temperature increased. The deposits in part interact strongly with the acid sites and block the sites for further alkylation reactions. Their structure and route of formation resemble those of conjunct polymers formed in liquid acid-catalyzed alkylation.

Keywords: Isobutane/butene alkylation; Zeolites; Deactivation; Coke analysis; MALDI; LDI

1. Introduction

Acidic large-pore zeolites are active and selective isobutane/butene alkylation catalysts [1,2]. Their industrial application is constrained by rapid deactivation with time on stream. The reaction proceeds mainly via addition of *n*-butene to an isobutyl carbenium ion. The resulting octyl carbenium ion is removed (after possible isomerization) from the active site by hydride transfer from isobutane leading to trimethylpentanes as ideal products and an isobutyl ion, which perpetuates the reaction. The overall scheme of this catalytic cycle is shown in Fig. 1. The main factor determining the fate of the catalyst is its hydride transfer activity. The higher the ratio of the rate of hydride transfer vs the rate of oligomerization, the more the primary products trimethylpentanes will be produced and the more the deactivation will be slowed down. Two strategies help to maximize hydride transfer rates: (1) Careful synthesis and modification procedures of the zeolites will minimize structural damage and ensure a high concentration of strong Brønsted acid sites, which effectively catalyze hydride transfer reactions. (2) The use of well-stirred tank reactors operated at very high conversions allows having a minimum local concentration of olefins, while maintaining high space velocities. This minimizes oligomerization activity, which is responsible for a low product quality and premature catalyst deactivation.

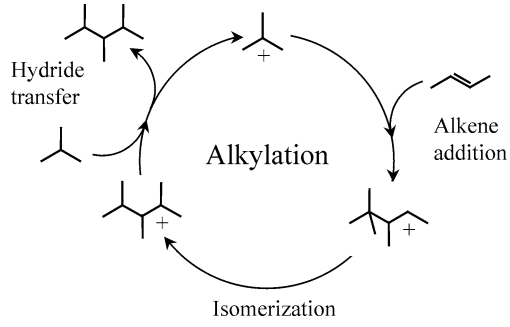

Fig. 1. Simplified alkylation reaction scheme.

Nevertheless, even under these conditions, deactivation of the catalyst occurs and it must be frequently regenerated. The patent literature suggests that multiple regenerations (as many as several hundred) are needed for processes based on solid catalysts to be competitive with existing processes based on H_2SO_4 and HF [3].

Thus, the understanding of the deactivation mechanism is important for prolonging the active single-cycle lifetime and for designing an efficient regeneration method. Only a small number of publications have been devoted to the characterization of carbonaceous deposits in zeolite-catalyzed isobutane/butene alkylation. The characterization techniques that were employed range from ^{13}C NMR [4–7], ^{1}H NMR [8],

* Corresponding author.
E-mail address: johannes.lercher@ch.tum.de (J.A. Lercher).

0021-9517/$ – see front matter
doi:10.1016/S0021-9517(03)00251-3

mass spectrometry (also in combination with gas chromatography) [8–10], IR-spectroscopy [6,8,11,12], and UV/VIS [6,13]. These methods were applied to the deactivated catalyst as a whole or to the extracted coke alone.

Coke extraction from zeolitic catalysts typically is done by a complete dissolution of the zeolite in aqueous hydrofluoric acid after which the coke is extracted with an organic solvent, e.g., hexane or methylene chloride. The carbonaceous compounds have been shown to survive this treatment unaltered [14].

Matrix-assisted laser desorption/ionization time-of-flight mass spectroscopy, MALDI-TOF and LDI-TOF MS, have been successfully applied as powerful techniques for the determination of the mass of polymers [15] and biomolecules [16]. Both methods utilize the energy of a laser beam for desorbing and ionizing sample molecules, which are subsequently analyzed in a time-of-flight mass spectrometer. In LDI-TOF, the sample itself is desorbed and ionized by the laser beam or postionized either by another laser or with an electron beam [17]. In MALDI-TOF, on the other hand, a matrix, typically an aromatic acid, is mixed with the sample. The matrix absorbs the laser power, is vaporized, and carries with it analyte molecules into the gas phase, where they can be ionized by protonation or cation addition or by charge transfer from the formed matrix ions. The different ionization mechanisms are discussed in Ref. [18]. The primary advantage of the laser desorption/ionization is the relatively low energy input, which minimizes fragmentation. Thus, the measured mass spectrum directly represents the molecular weight distribution of the analyzed mixture. In turn, however, this eliminates all structural information.

Recently, these methods have been successfully applied to the characterization of technical waxes [19], high-molecular-weight alkanes in crude oil [20], and low-molecular-weight hydrocarbon oligomers [21], all containing mainly aliphatic and naphtenic compounds with masses below 1000 Da. In principle, these mixtures should not be fundamentally different from the deposits formed on the catalysts during alkylation. For this reason, we developed these mass spectrometry methods for the characterization of the carbonaceous compounds and applied it to deactivated catalysts and on the free deposits.

In this communication, we seek to deepen the understanding of the deactivation mechanism. Analysis of reaction data obtained in a CSTR is combined with information on the deposits formed during the reaction and on the behavior of the deposits under thermal treatment. A variety of characterization techniques on the deactivated catalyst and on the extracted coke is used.

2. Experimental

2.1. Catalyst preparation

The parent material was Na-X obtained from Chemische Werke Bad Köstritz (Si/Al = 1.2). It was brought into the acidic form by aqueous exchange with 0.2 M lanthanum nitrate solution. The liquid-to-solid ratios in the exchange steps were usually approximately 10 ml/g. The temperature during exchange was kept at 70 °C and the exchange time was 2 h. This procedure was typically repeated 2–3 times. After washing the resulting material with doubly distilled water until it was nitrate-free and drying at 100 °C, the samples were calcined in flowing air with a slow temperature ramp up to 450 °C. To lower the sodium content of the zeolites further, this ion-exchange procedure including washing, drying, and calcining was repeated. The sample denoted La-H-X, was additionally exchanged with an ammonium nitrate solution (0.5 M) in this second step. The sample exclusively exchanged with La-ions was named La-X. For comparison, a sample of zeolite H-BEA (H-BEA 25 from Süd-Chemie, Si/Al = 12) was employed without further modification.

2.2. Catalyst characterization

The ion-exchanged zeolites were characterized by a range of different methods. With nitrogen adsorption in a PMI Automated BET Sorptometer at 77 K, surface area and pore volume were estimated. Prior to adsorption, the samples were activated in vacuum at 400 °C for 10 h. The crystallite size and morphology were analyzed with SEM. AAS was used to determine the Si/Al ratio and the Na^+ concentration. For measuring the acidity, two different kinds of adsorption/desorption experiments were carried out. To estimate the total number of acid sites (at an adsorption temperature of 100 °C) TPD of ammonia in a vacuum setup with a mass spectrometer detector (Balzers QMG 420) was performed. The strength and relative concentration of Brønsted and Lewis acid sites were characterized by sorption of pyridine monitored by IR spectroscopy using a Bruker IFS-88 FT-IR spectrometer equipped with a vacuum cell. For the latter the sample was pressed into a self-supporting wafer, which was placed into the vacuum cell, where it was activated in vacuum (10^{-5} mbar) for 1 h at 450 °C. Then, the sample was cooled down to 100 °C and pyridine at a partial pressure of 10^{-2} mbar was introduced into the system. After saturation of all the acid sites, the sample was outgassed for 1 h at 100 °C followed by a temperature ramp of 10 °C/min to 450 °C with a dwell time of 1 h. Subsequently, the cell was cooled down again to 100 °C. Spectra of the sample were taken before adsorption of pyridine, after outgassing and after desorption to 450 °C. All spectra were taken at 100 °C. From this set of spectra, the ratio of Brønsted acid sites (as evidenced by the band of pyridinium ions at 1540 cm^{-1}) to Lewis acid sites (the band of coordinately bound pyridine at 1450 cm^{-1}) at 100 °C and at 450 °C is calculated. The ratios of the extinction coefficients for Brønsted and Lewis bound pyridine were taken from Ref. [22].

2.3. Coke characterization

Coke was analyzed while adsorbed on the catalyst surface and after dissolution of the surrounding zeolite. For clarity, the former is denoted "deactivated catalyst" and the latter "free deposit." Deactivated catalyst samples were characterized by nitrogen adsorption at 77 K, after a vacuum treatment for 10 h at 120 °C to remove weakly bound compounds. These samples were compared to fresh zeolite samples also pretreated at 120 °C for 10 h, which is different from the pretreatment employed to estimate the overall surface area (see above). IR spectroscopy was used to characterize the hydrocarbon species on the deactivated catalysts by the individual bands that could be assigned to certain functional groups. For these measurements, wafers of deactivated catalysts were placed into the vacuum cell of the IR spectrometer and evacuated at 100 °C for 2 h, after which spectra were taken. Then, to measure the acid site distribution of the deactivated catalysts, pyridine was adsorbed following the same procedure as described with the fresh catalyst samples. Mass spectrometry was employed for monitoring the desorbing products during temperature-programmed desorption experiments of deactivated catalysts.

Matrix-assisted laser desorption/ionization time-of-flight mass spectrometry was used on the deactivated catalysts to obtain the molecular weight distribution of the hydrocarbon deposits. A solution of 1% trifluoroacetic acid in acetonitrile was prepared, and 10 mg of the deactivated catalyst was suspended in 100 µl of this solution. Another 100 µl of this solution was saturated with dihydroxybenzoic acid (DHB). The two parts were mixed and 0.5 µl of the resulting suspension was deposited on the sample holder. After air drying the drop, the sample holder was introduced into the ion source of the mass spectrometer. MALDI-TOF-mass spectra were recorded using a Bruker Biflex III MALDI-TOF mass spectrometer equipped with a N_2 laser ($\nu = 337$ nm) operating at a pulse rate of 3 Hz. The ions were accelerated with pulsed ion extraction after a delay of 50 ns by a voltage of 28.5 kV. The analyzer was operated in reflectron mode, and the ions were detected using a microchannel plate detector. The mass spectrometer was calibrated prior to measurement with a polystyrene standard of appropriate molecular mass. The same instrument was also used in laser desorption/ionization mass spectrometry. Here, the sample was suspended in water and put on the target without matrix. The experiments were conducted using the same settings as in the MALDI measurements. Supplementary experiments were performed with silver tetrafluoroborate ($AgBF_4$) added to the samples. This was supposed to lead to silver cationization of otherwise difficult to ionize alkanes.

For some measurements, the deposits had to be separated from the zeolite. This was done by a complete dissolution of the deactivated zeolite in a 40% hydrofluoric acid solution at room temperature. Unreacted HF was evaporated and the remainder was mixed with water and hexane and treated in ultrasound for 30 min. The brown colored hydrocarbon phase contained the deposits and was used for further analysis. The free deposits were characterized by UV/VIS in a Hitachi U-3000 spectrophotometer upon further dilution with hexane in the wavelength region 190 to 500 nm to obtain information on the olefinic and/or aromatic nature of the compounds. The free deposits were also analyzed by ^1H NMR at 360 MHz on a Bruker AM 360 spectrometer. After evaporation of the hexane solvent, the remaining tar-like polymer was redissolved in $CDCl_3$. Traces of $CHCl_3$ in the solvent were used as an internal standard for calibrating the chemical shift (δ $CHCl_3 = 7.24$ ppm from TMS). GC-MS in EI mode utilizing a OV-1 column was used to obtain information on the number and on the structure of the individual compounds. LDI mass spectra of the free deposits (with and without addition of $AgBF_4$) were taken and compared with mass spectra of the deactivated catalysts.

2.4. Catalytic experiments

The alkylation of isobutane with 2-butene was performed in a stirred tank reactor operated in continuous mode. The liquefied gases were received from Messer with a purity of 99.95% (isobutane) and 99.5% (*cis*-2-butene, the main impurity being *trans*-2-butene). Impurities in the feed cannot be completely ruled out to contribute to the catalyst deactivation. However, all known organic contaminants (diolefins, organic sulfur, and oxygen-containing compounds) were below the detection limit of our GC analysis. An estimation of the required concentration for a significant contribution of such a contaminant to catalyst deactivation would be about 50–100 times higher than the detection limit.

The catalyst sample (typically 4–5 g) was activated in situ within the alkylation reactor at 170 °C for 16 h in flowing nitrogen. After cooling to the reaction temperature, typically 75 °C, the reactor was filled with liquid isobutane at a pressure of 32 bar. The reaction was started by admitting a butene–isobutane mixture with a molar paraffin-to-olefin (P/O) ratio of 6.7 and an olefin space velocity (OSV) of 0.2 $g_{butene}/(g_{catalyst}\,h)$. Note that these numbers are comparable to industrially employed parameters. To study the influence of the reaction temperature on the deactivation process, a series of runs was performed at temperatures ranging from 40 to 130 °C.

The reactor was equipped with a sample valve, which allowed the removal of small amounts (ca. 20 mg) of catalyst on-line during the reaction. This mass loss was negligible for the overall run, being about 0.2–0.25% of the total catalyst inventory. Thus, during one reaction several samples could be withdrawn and analyzed for the progress of deactivation with time on stream.

The product from the reactor was expanded and passed through a six-port valve with a sample loop, the contents of which were injected automatically into an HP 6830 gas chromatograph equipped with a FID detector and a 35-m DB-1 column. Downstream of the six-port valve, the product stream was condensed into a cold trap cooled with a dry

Table 1
Physicochemical properties of the fresh catalysts

Sample	Total acid site concentration[a]	Brønsted/Lewis acid site ratio[b]		Micropore volume[c]	BET surface area[c]
	(mmol/g)	100 °C	450 °C	(ml/g)	(m^2/g)
La-X	0.67	3.5	2.9	0.16	505
La-H-X	0.55	2.3	1.6	0.16	518
H-BEA	0.50	0.9	0.2	0.07	566

[a] Measured by adsorption of ammonia at 100 °C.
[b] Measured by adsorption/desorption of pyridine monitored by IR.
[c] Measured by adsorption of nitrogen at 77 K after activation at 400 °C in vacuum for 10 h.

ice/isopropanol mixture. The product was collected over the whole time on stream and was weighed and analyzed chromatographically to give the integral product composition. The product was analyzed by UV/VIS and ^{1}H NMR. Additionally, an elemental analysis (by complete combustion) was performed on the product for obtaining the overall H/C ratio.

3. Results and interpretation

3.1. Physicochemical characterization

The most important physicochemical properties of the investigated catalysts are summarized in Table 1. The Na^+ content of all the samples was below 0.1 wt%. The crystal size of the faujasitic materials was between 1 and 2 µm. H-BEA sample had primary particles of about 0.1 µm, most of which were agglomerated to bigger aggregates.

3.2. Alkylation experiments

The three samples varied significantly in their alkylation performance. At a reaction temperature of 75 °C and employing an OSV of 0.2 $g_{butene}/(g_{catalyst}\,h)$ and a P/O ratio of 6.7, the time of complete butene conversion (termed catalyst lifetime) was 12 h for La-X, 9 h for La-H-X, and only 3 h for H-BEA. These differences can be attributed to the acidity distribution of the individual samples. La-X with the highest ratio of Brønsted to Lewis acid sites at both 100 and 450 °C is superior to La-H-X and H-BEA with their correspondingly lower ratios. La-H-X was additionally tested at a range of different reaction temperatures between 40 and 130 °C. The lifetime was found to be optimal at 75 °C, while higher selectivities to trimethylpentanes were achieved at lower temperatures. With all samples, the yield of products steadily increased with TOS, before it reached the theoretical limit of 2.04 $g_{product}/g_{olefin}$. When the conversion started dropping, the yield also declined. The results of these experiments are summarized in Table 2. The reported selectivities are based on the total amount of products that was produced until the activity to alkylation ceased. The implications of the acidity and the reaction temperature on the alkylation performance have been discussed in detail elsewhere [23].

Table 2
Lifetimes and integral selectivities measured in the different alkylation experiments at an isobutane/2-butene ratio of 6.7 and 2-butene space velocity of 0.2 g/(g h)

Sample	Reaction temperature (°C)	Lifetime (h)	Product group selectivities (wt%)			
			C_5–C_7	TMP	DMH	C_{9+}
La-X	75	12	18.3	57.8	14.1	9.8
H-BEA	75	3	16.0	57.4	12.2	14.3
La-H-X	40	2	9.8	71.5	10.1	8.6
	75	9	14.7	64.2	13.4	7.7
	100	6	25.3	49.1	14.7	10.9
	130	2	35.0	29.9	18.6	16.4

3.3. Characterization of the deactivated catalysts

Samples of the deactivated catalysts La-X and H-BEA were analyzed by IR spectroscopy. Spectra were taken at 100 °C after outgassing at 100 °C in vacuum for 2 h. The spectra of the two deactivated catalysts are compared in Fig. 2. Both samples showed the typical bands for sorbed hydrocarbons. The bands at 2960 and 2930 cm^{-1} are characteristic of the asymmetric stretching vibrations of the CH_3 and the CH_2 group, respectively. The different intensities of these two bands in the two samples indicate a higher degree of branching of the hydrocarbons present on La-X. The bands at 1465 and 1380 cm^{-1} are attributed to the asymmetric and symmetric CH_3 deformation vibration. The band at 1640 cm^{-1} is assigned to the stretching mode of a C=C double bond. The samples were exposed to atmospheric conditions after removing them from the reactor. Thus, it cannot be completely ruled out, that the band at 1640 cm^{-1} is partly caused by the deformation vibration of adsorbed water, usually found between 1630 and 1610 cm^{-1}. With La-X a weak band at 1536 cm^{-1} is observed, and with H-BEA two stronger bands at 1531 and 1505 cm^{-1} are observed. Hydrocarbon bands in this region were assigned to alkenyl cations in both liquid acids [24,25] and zeolites [26,27]. However, also partly oxidized species such as carboxyl groups absorb around 1600 and 1530 cm^{-1}. Bands characteristic of aromatic molecules were not detected. Let us now consider the bands of the hydroxy groups. With La-X, all bands of acidic hydroxy groups including the SiOH band are completely missing and only the band at 3520 cm^{-1} characteristic of the nonacidic La–OH band was observed. In contrast with H-BEA a fraction of the silanol (3740 cm^{-1}) and the acidic hydroxyl band (3605 cm^{-1}) is visible and, hence, not covered by hydrocarbons.

A sample of deactivated La-X was used to study the behavior of the hydrocarbon deposits during thermal treatment. After outgassing at 100 °C, the temperature was raised with 10 K/min to 450 °C. A mass spectrometer connected to the IR cell recorded the desorbing species. Fig. 3 shows the IR spectra taken before and after the thermal treatment in comparison with the fresh sample and the evolution of the bands during the temperature increase. All hydrocarbon bands decrease in intensity with increasing temperature. This de-

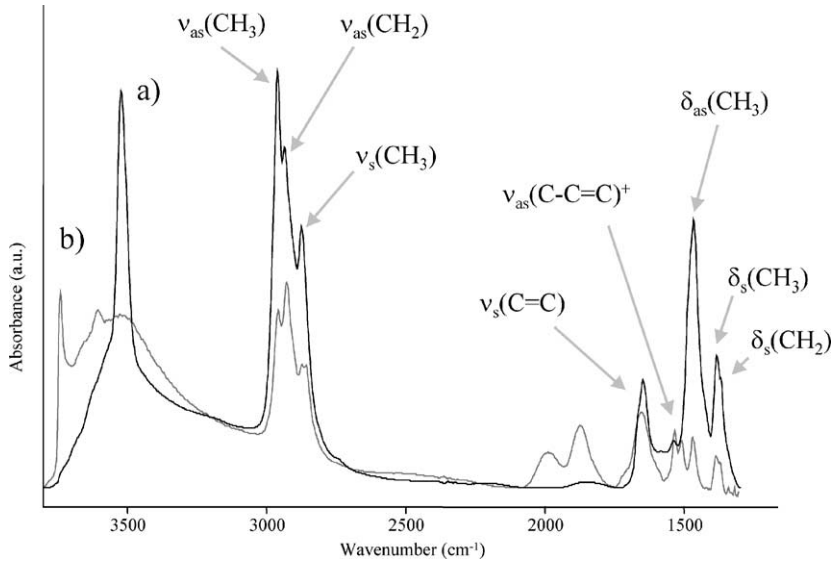

Fig. 2. Spectra of deactivated catalysts (alkylation at 75 °C) after evacuating for 2 h at 100 °C with assignment of hydrocarbon bands. (a) La-X (black line), (b) H-BEA (gray line).

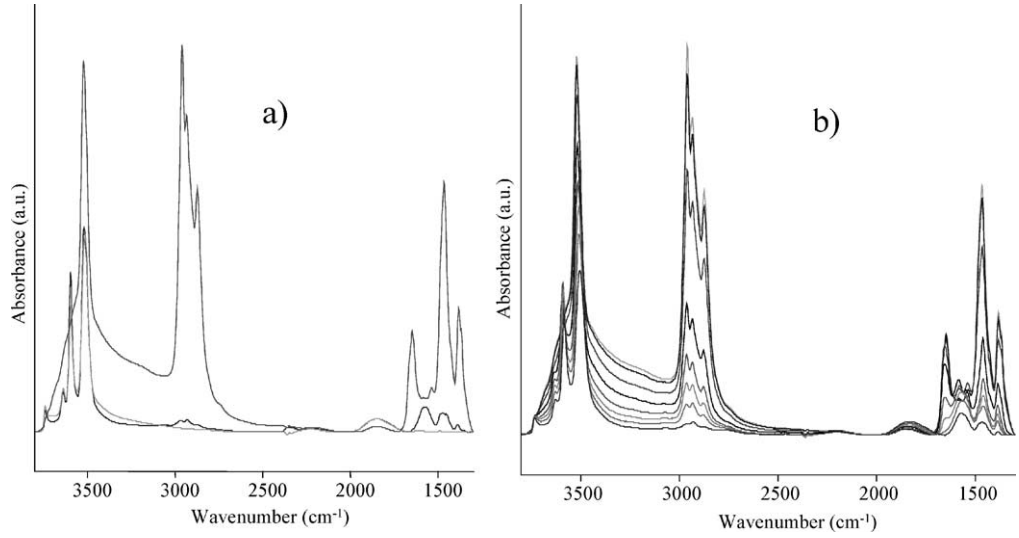

Fig. 3. Thermal treatment of deactivated catalyst La-X recorded with IR. (a) Comparison between fresh sample, deactivated sample after outgassing at 100 °C, and after heating to 450 °C, (b) Changes during heating to 450 °C. Spectra were taken every 50 °C, starting from 100 °C.

crease is accompanied by the appearance of a new band at 1580 cm^{-1}, which is tentatively assigned to condensed ring aromatic structures [14] or structural vibrations of polycyclic aromatic compounds [28]. A weak band at 3070 cm^{-1} characteristic of the C–H stretching vibration of aromatic compounds supports this assignment. Only weak bands were observed between 3000 and 2700 cm^{-1} after thermal treatment. In the region between 1700 and 1300 cm^{-1} the CH_3 bending vibrations were markedly reduced in intensity. The intensity and shape of the hydroxyl bands of the sample after the thermal treatment were similar to those of the fresh sample.

The species desorbing during the thermal treatment can be grouped into two categories, i.e., alkanes and alkenes that desorbed between 100 and 280 °C, and the high temperature desorption of aromatic compounds starting at 250 °C. Fragments characteristic of the different types of molecules desorbing from the zeolite surface are compiled in Fig. 4. The masses 83 and 85 represent alkene and alkane fragments. Mass 119 represents aromatic compounds with one benzene ring (substituted with alkyl side chains) and mass 115 represents bicyclic aromatics, which desorb at temperatures above 300 °C.

The alkylation reaction was also simulated in an IR flow cell. The sample was activated at 450 °C in the cell in a stream of helium before a flow of a gaseous mixture of isobutane/2-butene (P/O = 6.7) was passed over the catalyst at 75 °C. Immediately, the acidic hydroxyl bands disappeared and the bands typical for hydrocarbons evolved. Although the flow was maintained for 75 min, the hydrocar-

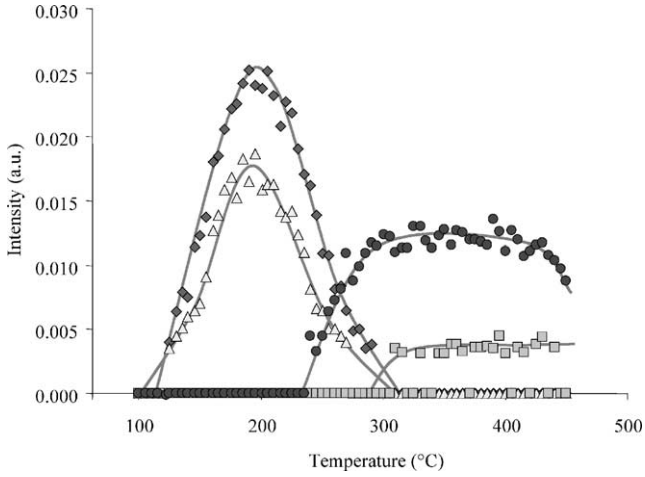

Fig. 4. Temperature-programmed desorption of hydrocarbons from deactivated catalyst La-X monitored by MS. ◆, mass 83; △, mass 85; □, mass 115; ●, mass 119.

bon band intensities reached a plateau after the first 10 min. Next, the sample was flushed with He for 180 min at 100 °C. The spectrum taken after this treatment looked very similar to the spectrum of the deactivated catalyst (Fig. 2a) with the following differences: (1) the silanol band was still visible in the spectrum of the sample exposed to the alkylation reagents in the IR reactor and (2) the bands in the 1500–1540 cm^{-1} region were missing in this spectrum.

The remaining acidity of deactivated zeolites La-X and H-BEA was analyzed with pyridine adsorption at 100 °C in the IR cell. Prior to adsorption, the samples were outgassed at 100 °C in vacuum for 2 h. In Fig. 5, difference spectra of adsorbed pyridine on the fresh zeolites in comparison to the deactivated zeolites are shown. In both samples, pyridine could access a large fraction of the originally present Brønsted acid sites and a smaller fraction of the Lewis acid sites. Additionally, the hydrocarbon bands at 1650, 1530, 1505, and 1470 cm^{-1} were reduced in intensity after pyridine adsorption.

The deactivated zeolites La-X and H-BEA were also analyzed by nitrogen adsorption. Here, the fresh and used samples were pretreated at 120 °C for 10 h in vacuum. Especially with the hydrophilic La-X, this is too low to completely remove the strongly sorbed water from the fresh sample, but most of the micropore area is accessible for nitrogen. After pretreatment at 400 °C, a micropore volume of 0.16 ml/g was measured (see Table 1), and after pretreatment at 120 °C a micropore volume of only 0.09 ml/g. The results are displayed in Fig. 6. The micropores of the deactivated materials were completely blocked. Only a small fraction of the macro- and mesopores were accessible for N_2. It should be emphasized that although outgassing was done at a slightly higher temperature and for a longer time, N_2 (in contrast to pyridine) did not access the micropores.

3.4. Characterization of the free deposits

The free deposits gained from La-H-X alkylated at different temperatures were analyzed with UV/VIS spectroscopy. The results are compiled in Fig. 7. Due to the unknown concentration and extinction coefficients of the individual compounds, the results are discussed only in qualitative terms. All spectra show a broad complex absorbance between 200 and 450 nm with three components at 200–205, 235, 250–260, and 310–320 nm. The energies strongly suggest the presence of π-electron systems in the deposits.

π-Electron systems of pure hydrocarbons, which absorb in this range, belong to single and conjugated double bonds or to C=C bonds in aromatic molecules. The breadth of the absorbance band suggests a high number of different but related species. The deposits recovered from the catalyst tested

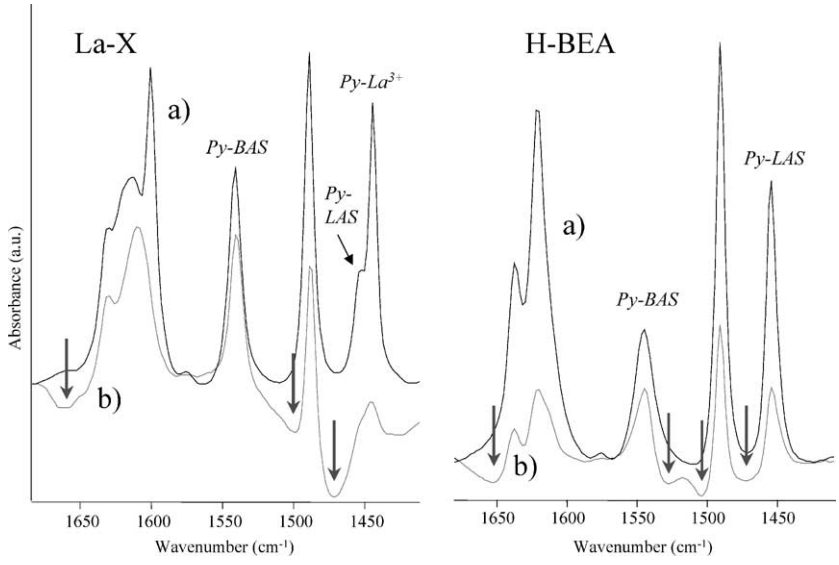

Fig. 5. Difference spectra of adsorbed pyridine on La-X and H-BEA in (a) fresh and (b) deactivated state at 100 °C. The arrows indicate the positions of the hydrocarbon bands, which were reduced in intensity upon adsorption of pyridine.

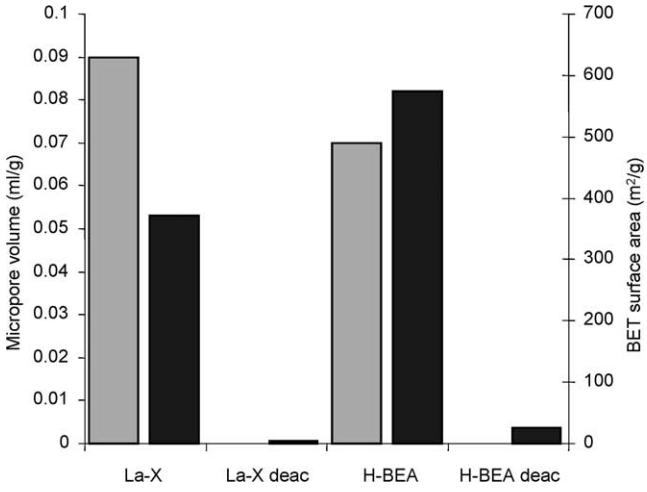

Fig. 6. Nitrogen adsorption at 77 K on La-X and H-BEA, in both fresh and deactivated states (after evacuation at 120 °C for 10 h). ▭, Micropore volume (left axis); ■, BET surface area (right axis).

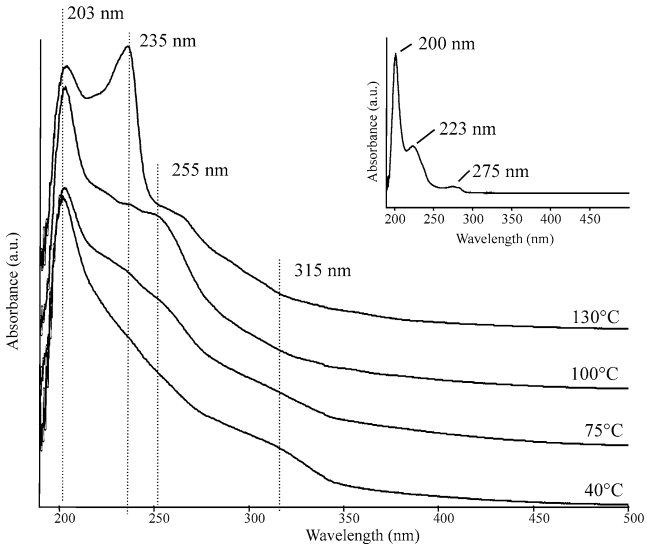

Fig. 7. UV/VIS spectra of the free deposits dissolved in hexane gained from alkylation runs of La-H-X at different reaction temperatures. Inset shows the UV/VIS spectrum of the heavy-end fraction of the alkylation product collected during the first 4 h TOS of a catalytic run with La-X.

at 130 °C, however, differed distinctively from the others. The absorbance at 235 nm, which is present in the other spectra only as a small shoulder, is the most prominent peak in the spectrum of the deposit from the reaction at 130 °C.

Shown as an inset in Fig. 7 is the UV/VIS spectrum of the heavy-end fraction (hydrocarbons in the alkylate with nine or more carbon atoms, C_{9+} fraction) of alkylate collected over the first 4 h of time on stream with La-X as catalyst. During this period, the catalyst exhibited 100% butene conversion. Typically, only very small amounts of alkenes (especially octenes) are found in the products during the initial reaction phase. The integral selectivity of alkenes in the C_5–C_8 fraction is in the order of 0.2 wt%. Information on the concentration of unsaturated compounds in the C_{9+} fraction is not available. The UV/VIS spectrum revealed the presence of unsaturated and/or aromatic species. The spectrum shows sharper bands than that of the free deposits, suggesting a lower number of different compounds. Additionally, the product does not absorb at wavelengths above 300 nm.

The GC-MS measurements of the free deposits established their highly branched nature at all reaction temperatures. In many spectra the mass fragment 57 ($C_4H_9^+$) exhibited the highest peak. Independent of the reaction temperature, the compounds at higher retention times were more and more hydrogen deficient. The number of substituted benzene (evidenced by the mass fragments 77, 91, and 105) and condensed aromatic species (mass fragments 115 and 129, most likely containing no more than 3 rings) was very low in the deposit formed at 40 °C, slightly higher in the deposit formed at 75 °C, and substantially higher in the deposit formed at 130 °C. The reverse trend was seen for nonaromatic cyclic compounds containing 5- and/or 6-ring structures (discernible by the mass fragments 121, 123, and 124), which were more frequent in the deposits formed at 40 and 75 °C. Masses up to 490 m/z corresponding to C_{35} molecules were detected in all samples. Iso-alkane and alkene fragments were abundant in all samples, but in most of these spectra no molecular ion peak was present.

Molecular ion peaks found in the deposit formed at 40 °C mainly belonged to C_nH_{2n-2}-type compounds, to a lesser degree also to C_nH_{2n-4} and C_nH_{2n}. The deposit formed at 75 °C exhibited C_nH_{2n-2} and C_nH_{2n-4} compounds and at higher retention times also C_nH_{2n-6} and C_nH_{2n-8}. The deposit formed at 130 °C contained substances with markedly higher unsaturation, i.e., mainly C_nH_{2n-8}, some C_nH_{2n-6} and at higher retention times also C_nH_{2n-10} and C_nH_{2n-12}. Most of the molecular ion peaks were found in the C_{18}–C_{30} region for all deposits.

The free deposits formed at 40, 75, 100, and 130 °C were also analyzed by ^{1}H NMR spectroscopy. Additionally, two heavy-end fractions of reaction products were analyzed. One was accumulated over the first 4 h of time on stream, the other over the whole reaction time including the deactivation phase. The NMR spectra of the deposits are displayed in Fig. 8, those of the products in Fig. 9.

The peaks in each spectrum can be grouped to distinguish protons in different positions. This is only an approximate classification, because some of the functional groups overlap in their chemical shifts, depending on the surrounding groups. The signal between 0 and 1.1 ppm, which was most abundant in all spectra, corresponds to protons in CH_3 groups in α position to saturated C atoms. Its contribution to the overall signal was significantly higher in the alkylate samples than in the deposits. Thus, we conclude that the degree of branching was higher in the product than in the deposits. The degree of branching in the product at early TOS was higher than that of the product collected during the whole run including deactivation. The degree of branching in the deposits also continuously decreased with increasing

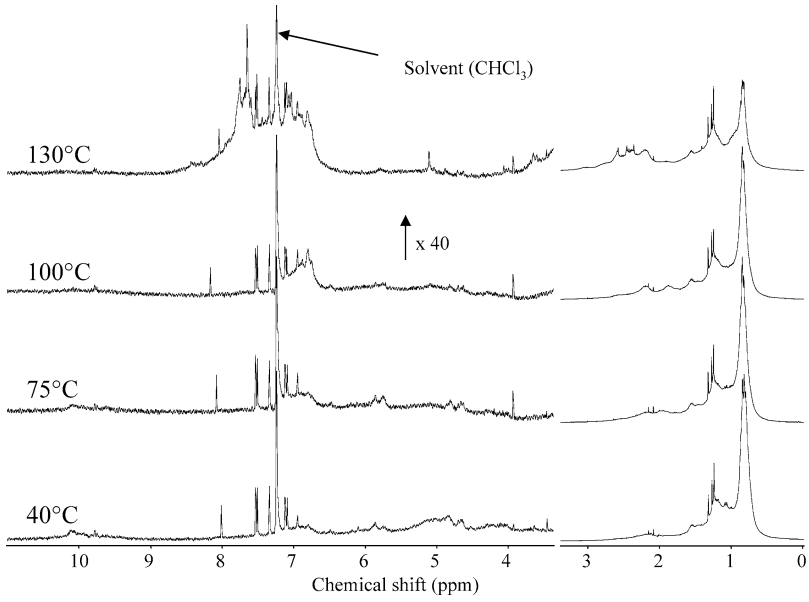

Fig. 8. ^{1}H NMR spectra of the free deposits recovered from La-H-X after alkylation at 40, 75, 100, and 130 °C.

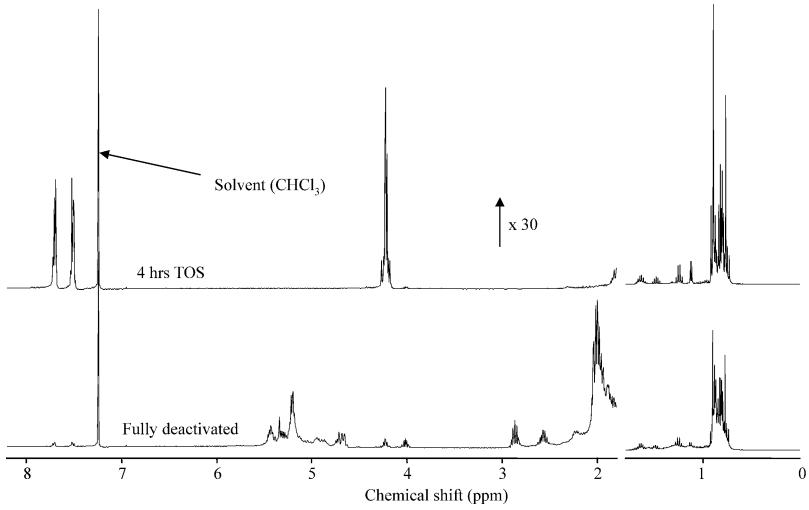

Fig. 9. ^{1}H NMR spectra of the heavy-end fractions of alkylates collected over the first 4 h TOS and after complete deactivation.

reaction temperature (the fraction of CH_3 protons decreased from 61% at 40 °C to 33% at 130 °C).

Signals between 1.1 and 1.4 ppm correspond to protons in CH_2 groups. No marked changes were seen in this group among the deposits (19–21%), whereas the product collected at early TOS showed only half the amount than the product collected during the whole run (6 and 14%). Signals between 1.4 and 1.7 ppm correspond to protons in CH groups in α position to saturated C atoms. With reaction temperature and reaction time the importance of this group increased (from 7 to 14% in the deposits and from 7 to 9% in the products).

Signals between 1.7 and 3.5 ppm represent protons in CH_3, CH_2, and CH groups in α position to unsaturated or aromatic carbon atoms. Due to the broad distribution of chemical shifts for these kinds of protons, a further classification within this range was not attempted. The number of protons in the deposits in this range increased steeply with reaction temperature (from 10% at 40 °C to 30% at 130 °C). Its contribution to the total number of protons in the products was much smaller (0.1 and 0.9%).

Protons of olefinic groups are found between 4 and 6.6 ppm. The deposits exhibited ill-resolved peaks in this range. Around 1.5% of all the protons in the deposits formed between 40 and 100 °C were located at olefinic carbon atoms. The deposit formed at 130 °C contained markedly less, only about 0.4%. The product collected during the complete run showed a broad absorption between 4.5 and 5.5 ppm. The product collected during the early reaction stage exhibited one sharp signal at 4.2 ppm. This peak most likely does not represent olefinic protons as will be discussed below.

Aromatic protons give resonances in the range 6.6 to 9 ppm. All deposits showed signals in this range, but the

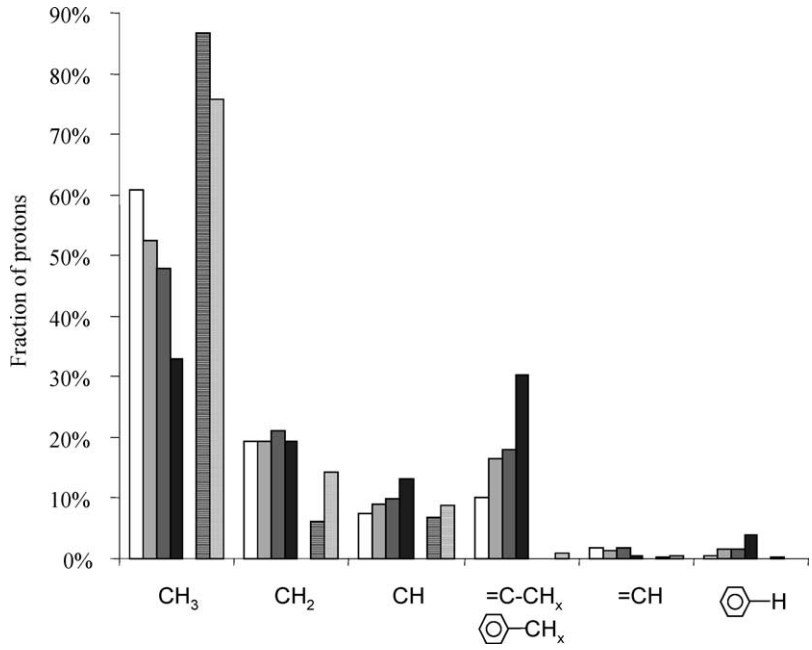

Fig. 10. Fraction of protons in the individual positions obtained by the integration of the NMR spectra in Figs. 8 and 9. □, 40 °C; ▒, 75 °C; ▒, 100 °C; ▒, 130 °C; ▒, heavy-end fraction of alkylate after 4 h TOS; ▒, heavy-end fraction of alkylate after complete deactivation.

amount steeply increased with increasing reaction temperature (from 0.5% at 40 °C to 3.9% at 130 °C). The products showed two sharp signals at 7.7 and 7.5 ppm, with a higher contribution in the product collected during the early reaction stage (0.2 and 0.04%). The signal at 4.2 ppm is proportional to them and is tentatively described to protons in a CH or CH_2 group connecting two aromatic rings. The lack of signals higher than 8.1 ppm in the spectra of the deposits formed from 40 to 100 °C suggests the absence of condensed aromatic molecules with three or more rings. The deposit formed at 130 °C might contain a small amount of these compounds. The number of protons in the deposits connected to carbon in α positions of olefinic or aromatic double bonds is 5–7 times higher than the number of protons within the double bonds. This demonstrates that these bonds are highly substituted.

Small contributions between 9.5 and 10.5 ppm seen in the low-temperature deposits were assigned to hydrogen in OH- or aldehyde groups. These could possibly result from oxidation reactions after the deposit had been exposed to air. An overview about the importance of each class of protons in the deposits and products is presented in Fig. 10.

The elemental analysis of the reaction products gave H/C ratios between 2.12 and 2.15, corroborating the almost pure paraffinic nature of the heavy-end alkylate.

3.5. MALDI-TOF mass spectrometry

In MALDI-TOF mass spectrometry typically protonated or cationized (typically by Na^+ or K^+) ions are detected. Acidic matrices such as DHB preferentially give protonated ions. In some special cases ionization through charge transfer or multiphoton ionization (leading to radical cations) may occur. In general, polar heteroatom-containing compounds are easier to ionize than pure hydrocarbons. Within the group of pure hydrocarbons, compounds with π-electron systems, such as aromatics, are easier to ionize than those without. Saturated hydrocarbons can only be ionized by the addition of silver cations, to which they form adducts [29]. From the NMR results it is known that the examined deactivated catalysts contain species of all these groups: alkanes, alkenes, aromatics, and in the case of the low-temperature deactivated catalysts also traces of oxidized products. MALDI is known to be able to detect very small traces in the ppb range, so it cannot be ruled out that the measured spectra represent minority species, which are especially easy to desorb and ionize.

Deactivated catalysts used in reactions at 40, 75, and 130 °C were analyzed by MALDI-TOF MS employing DHB as matrix. The mass spectra are displayed in Fig. 11. The samples from reactions at 40 and 75 °C resulted in very similar spectra. Both gave a clean Gaussian-curved distribution of masses with peaks in the mass range from 150 to 450 and a maximum between 235 and 291. A repetitive pattern was found within these samples. One prominent peak was always accompanied by a small peak 1 m/z higher and by a small peak 2 m/z below. This pattern was repeated every 14 m/z. This is a sign for each set being larger by a CH_2 group than the preceding set. For reasons not yet known, every forth of these sets exhibited a higher intensity than the Gaussian distribution. The main peaks based on the series $179 + 14n$. The detected species can be either protonated or cationized. Assuming the detected ions to be of the typical $[M+H]^+$ nature (which leads to uneven masses for hydrocarbons), this would correspond to molecules of a general C_nH_{2n-4} (three

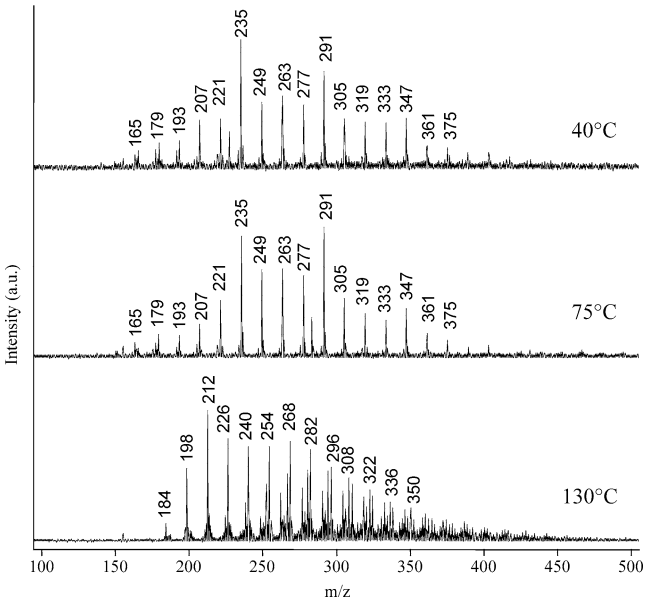

Fig. 11. MALDI-TOF mass spectra of the deactivated catalysts used in reactions at 40, 75, and 130 °C.

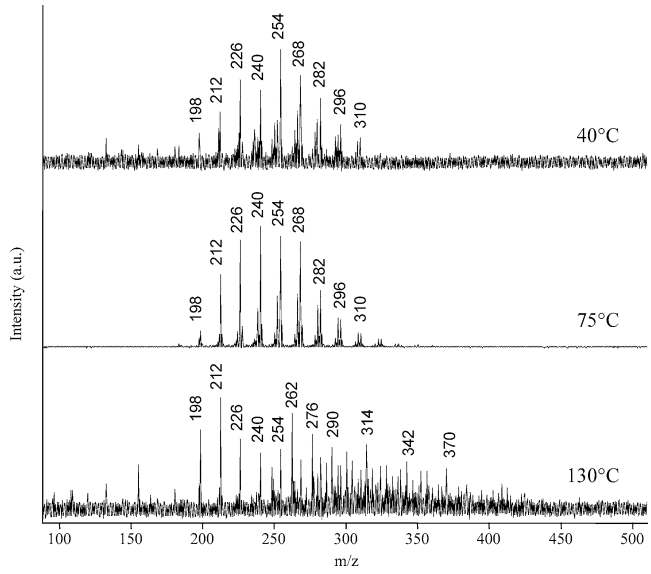

Fig. 12. LDI-TOF mass spectra of the deactivated catalysts used in reactions at 40, 75, and 130 °C.

unsaturations or cycles) or C_nH_{2n-18} (e.g., three condensed aromatic rings with alkyl side chains) formula. However, the matrix $[M + H]^+$ peak at 155 was nearly completely suppressed, which is typical for readily ionizable heteroatom-containing analytes [30]. Therefore, it is concluded that the detected ions originate from the oxidized products, possibly of a $C_nH_{2n-6}O$ structure.

The deactivated catalyst of the reaction at 130 °C gave a different spectrum. The mass distribution had a maximum at 212 m/z and then followed the distribution of the other spectra with a second maximum at 268 m/z. The main peaks were based on the $184 + 14n$ series. At higher molecular weights, additional series developed, being 2 and 6 m/z lower than the main series. At molecular weights above 300, these peaks showed higher intensities than the main series. At m/z above 330, series 4 and 8 m/z lower than the main series were seen. All these peaks represent *even* molecular masses in contrast to the MALDI spectra of the two other samples. Because of this, the signals cannot represent protonated or cationized hydrocarbons, which would always give uneven masses. It is therefore assumed that they (similar to LDI, see below) originate from radical cations. They represent molecules of the general formula C_nH_{2n-12}, C_nH_{2n-14} (or C_nH_{2n}), and C_nH_{2n-18} (or C_nH_{2n-4}). The C_nH_{2n-12} structures have the same molecular weight as alkanes. The occurrence of alkanes in the mass spectrum can be ruled out, because they cannot be ionized without the help of silver cations. Simple olefins also should be difficult to ionize. It is more likely that the detected masses represent the general formulas C_nH_{2n-14} and possibly also C_nH_{2n-18} rather than C_nH_{2n-4}.

The LDI-TOF mass spectra of the deactivated catalysts used in reactions at 40, 75, and 130 °C are displayed in Fig. 12. The mass distributions of the recorded spectra resembled the distributions measured by MALDI-TOF MS. They were narrower but centered on a similar maximum. The main peaks in all spectra were *even* masses. In the mass spectra of the catalysts deactivated at 40 and 75 °C the main peaks followed the $212 + 14n$ series, with smaller peaks 2 and 4 m/z below. They corresponded to the general formula C_nH_{2n-12}, C_nH_{2n-14}, and C_nH_{2n-16} (or C_nH_{2n-2}), respectively.

The LDI-TOF mass spectrum of the catalyst deactivated at 130 °C resembled the corresponding MALDI-TOF mass spectrum not only in the shape of the mass distribution curve but also in the detected masses themselves. Up to 250 m/z, peaks of the C_nH_{2n-12} series dominated as in the MALDI-TOF spectrum and as in the two other LDI spectra. Between 250 and 300 m/z, C_nH_{2n-18} (or C_nH_{2n-4}) were the main peaks, which were replaced by the C_nH_{2n-22} (or C_nH_{2n-8}) series above 300 m/z. This last series was nonexistent in the MALDI-TOF mass spectrum and in the other LDI-TOF mass spectra.

Typical MALDI spectra exhibit protonated molecular cations or analyte-cation adducts, the cation typically being Na^+ or K^+. For aliphatic hydrocarbons this should always lead to uneven masses. The molecules desorbing from the low-temperature-deactivated catalysts followed this rule; the one deactivated at 130 °C did not. Moreover, the MALDI spectrum of the high-temperature-deactivated catalyst was similar to the LDI spectra of the deactivated samples. This suggests that the majority of the detected masses were not ionized by the interaction with the matrix, but, as in LDI, ionized by the laser beam. All types of species, except for the oxidation products, found in the low-temperature deposits are also found in the high-temperature deposit. For this reason it is postulated that MALDI selectively ionizes oxygen-containing compounds (polar heteroatom-containing hydrocarbons are much easier to ionize than nonpolar pure hy-

drocarbons), which suppress the formation of other ions. In the absence of a matrix, only molecules with absorption in the region of the wavelength of the laser ($\lambda = 337$ nm) can be desorbed and ionized. The compounds are adsorbed on the zeolite surface and at least a fraction of them interacts strongly with the acid sites. It has been shown by Flego et al. that adsorbed species in deactivated zeolitic alkylation catalysts give rise to strong UV/VIS absorption bands between 300 and 400 nm assigned to alkenyl cations [6]. Unsaturated carbenium ions have been extensively examined by Deno and co-workers, who measured absorption bands in this range [25,31]. Flego et al. did not take into account that also aryl and benzenium cations exhibit absorption maxima between 300 and 400 nm [32]. Exhibiting even masses in the LDI spectra, these ions obviously desorb as the radical cations of the corresponding olefinic and aromatic molecules.

LDI mass spectra of the free deposits were also taken. This was unsuccessful for the deposits from the reactions at 40 and 75 °C, in which ions were not detected. The free deposit from the reaction at 130 °C readily gave a mass spectrum, resembling the LDI spectrum of the deactivated catalyst. Masses of the formula C_nH_{2n-12}, C_nH_{2n-14}, and C_nH_{2n-18} already seen in the deactivated samples were outweighed by masses of the formula C_nH_{2n-8} (or C_nH_{2n-22}) and C_nH_{2n-10} (or C_nH_{2n-24}). These results confirm the hypothesis that by LDI on the low-temperature-deactivated catalysts only unsaturated carbenium ions with sufficient absorption at 337 nm can be detected. None of these are present in the free deposits; therefore, no molecules are desorbed and ionized.

It is unclear at present why the free deposit formed at 130 °C led to the LDI peaks observed. The UV/VIS spectrum (see Fig. 7) did not show a significantly higher absorption at 337 nm than the other deposits. One possible explanation can be derived from studies by Macha et al., who examined the behavior of several nonpolar matrices (anthracene, acenaphthene, and similar aromatics with two to four condensed rings and sufficient absorption at 337 nm) and analytes (with low absorption at 337 nm) under MALDI conditions. The matrices were found to ionize the analyte molecules only when the ionization energy of the analyte was lower than the ionization energy of the matrix. In this way, the analyte is ionized by charge transfer from the matrix giving a molecular radical cation (and not by protonation) [33].

The unusual behavior of the high-temperature deposit is interpreted accordingly. The aromatic fraction of the free deposit might contain a sufficiently large amount of molecules acting as matrices for compounds that otherwise would not be ionized due to lack of absorption at 337 nm. The same molecules in the low-temperature deposits with their significantly lower proportion of aromatics cannot be ionized because of the absence of suitable matrices.

Silver salts are frequently used to ionize alkanes and cycloalkanes by forming cation adducts in MALDI and LDI MS [21]. The addition of $AgBF_4$ to the deactivated catalysts containing DHB as matrix only led to a considerable decrease in signal intensity without changing peak positions. No silver adducts were detected. Adding $AgBF_4$ to the deactivated catalysts without a further matrix gave mass spectra, which contained the uneven masses seen in MALDI mode and the even masses observed in LDI mode. Also here no silver adducts were detected. Therefore, it is tentatively concluded that the silver salt or metallic silver (the silver salts readily decompose) may act as a matrix itself.

Fine metal or metal oxide powder has also been successfully employed as matrix for small molecule analysis leading to protonated or alkali–adduct ions [34]. The matrix effect is weaker as with DHB, because the formation of "LDI-type ions" is not fully suppressed. The same was observed with the deposits. Mixing the low-temperature deposits with $AgBF_4$ gave the typical "MALDI-type ions" with strongly reduced signal intensity. The high-temperature deposit gave the same spectrum as without silver addition. Again, silver adducts were not detected.

The molecular weight distribution measured with MALDI and LDI MS gave the same maximum at 260–270 m/z. The LDI mass spectra were narrower than the MALDI spectra. MALDI gave masses between 150 and 450 m/z, LDI between 190 and 340 and 420 m/z for the catalyst deactivated at 130 °C. The LDI mass spectrum of the deposit formed at 130 °C had a distribution between 220 and 510 m/z. The maximum was also shifted to 314–328 m/z. Molecules at the lower end of the molecular weight distribution might evaporate in the ultra high vacuum of the MALDI apparatus when not adsorbed on the zeolite, so that the maximum is seen at higher masses. Moreover, it is not known whether the mass distribution of the deposits on the outer surface of the zeolite is different from the distribution within the pores. The laser can only desorb molecules on or close to the outer surface of the zeolite particles.

During reaction on La-H-X at 75 °C, catalyst samples were withdrawn at 3.75, 6.7, and 9 h TOS. These samples were analyzed by MALDI to examine the progress of catalyst deactivation. All three samples exhibited spectra similar to the one shown in Fig. 11. The mass spectrum taken after 3.75 h TOS exhibited a maximum in the mass distribution, which was approximately 50 m/z lower than the maxima of the spectra taken after 6.7 and 9 h TOS. With time on stream the signal intensity increased. While there was only a moderate increase up to 6.7 h TOS, it steeply increased when the catalyst reached the end of its active lifetime, see Fig. 13.

4. Discussion

4.1. Chemical nature of the deposits

While MALDI/LDI-TOF-MS (Figs. 11 and 12) gives information on the molecular mass distribution of the mole-

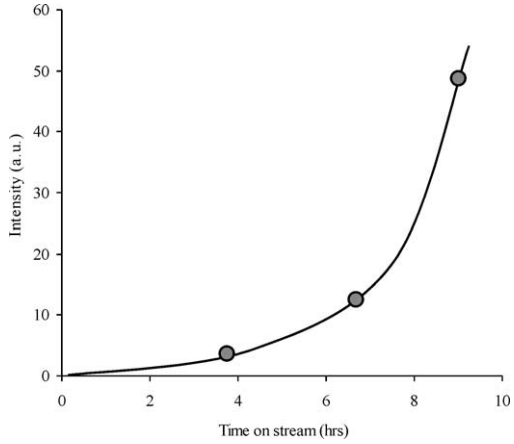

Fig. 13. Signal intensity of MALDI-TOF mass spectra taken at different times on stream during reaction on La-H-X at 75 °C.

cules in the deposits, NMR (Fig. 8) and UV/VIS (Fig. 7) (although to a lesser degree) give information on the structure of the molecules. GC-MS provides useful information on both the mass and the structure. UV/VIS and LDI clearly proved that all deposits contained unsaturated species. However, both methods cannot detect saturated hydrocarbons. The significance of the unsaturated compounds can be estimated from NMR and GC-MS. Both these methods revealed an increase in the concentration of unsaturates as well as an increase in the degree of unsaturation with increasing reaction temperature. This increase was gradual at low to moderate temperatures and steep toward high reaction temperatures. However, at all reaction temperatures, the deposit is a complex mixture of alkanes, alkenes, and nonaromatic cyclic and aromatic compounds, all of them with alkyl side chains. Polycyclic aromatics were found only at high reaction temperatures. For low to moderate temperatures, MALDI, LDI, and GC-MS gave a carbon number distribution in the range of C_{12}–C_{35}, with a maximum at about C_{20}. These numbers slightly shifted to higher values at high reaction temperatures.

Our detection of unsaturated species is in line with results obtained via mass spectrometry analysis of extracted coke performed by two different research groups [8,9]. C_{15}–C_{20} compounds with 2–4 unsaturations/cycles were found in the deposits. After hydrogenation, the general formula suggested a naphtenic structure with one or two 5 and 6 rings. UV/VIS data obtained by Flego et al. also confirmed the unsaturated nature of the deposits [6].

These unsaturated cyclic structures are very similar to the so-called conjunct polymers, which are by-products of sulfuric and hydrofluoric acid-catalyzed alkylation reactions. The polymers are dissolved in the acid phase and are responsible for the acid consumption due to the decrease of the acid strength [35,36]. The conjunct polymers were shown to be cyclic polyolefinic hydrocarbons with a high proportion of heteroannular-conjugated double bonds and numerous side chains [37].

4.2. Routes of formation of coke compounds

The deposits in alkylation often have been intuitively related to large saturated species that result from multiple alkylation and oligomerization of butenes and other alkenes formed during the alkylation reaction [4,5,7]. The results presented here demonstrate that the products retained in the zeolite pores during isobutane/butene alkylation are complex and strongly vary with subtle variations in the reaction conditions. Only a fraction of the detected compounds originates from the typical alkylation reactions. The detected alkanes are products of multiple alkylation, similar to the heavy-end fraction of the reaction products. The molecules are probably too bulky to diffuse out of the pores. Alkenes found in the deposits are concluded to originate from alkoxides bound to the acid sites in the zeolite pores.

All other compounds have to undergo additional reactions. As a start, a large cation produced via multiple alkylation or oligomerization has to crack or deprotonate to form a large and branched alkene. This might transfer a hydride to another carbenium ion and, thus, form an alkenyl carbenium ion, which can desorb via proton transfer as a diene (Scheme 1). Further hydride transfer leads to a dienylic cation, which easily rearranges into an alkyl-substituted ring (Scheme 2) via a 1,5-cyclization and subsequent hydride and methyl shifts. Next to the ion, also a saturated molecule (represented here as isobutane) is produced in each step. Therefore, no true dehydrogenation step is involved.

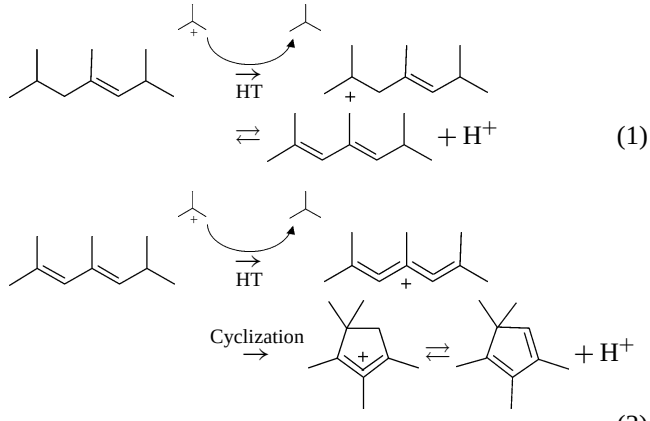

The formed cycloalkenyl carbenium ions, especially the cyclopentenyl cations, are very stable [25,38] and have been observed as free cations in zeolites [39,40]. The occurrence of enylic cations was established by the IR bands between 1540 and 1500 cm^{-1}. The same reaction sequence is operative when absorbing alkenes in concentrated sulfuric acid. The alkenes disproportionate on the one hand into a layer of saturated hydrocarbons, and on the other hand into highly unsaturated cyclic compounds dissolved in the acid phase, which turns a dark red color [41,42].

Gas-phase alkylation did not lead to the formation of alkenyl ions. This is seen in the absence of bands in the region 1500–1540 cm^{-1}. We explain this with the lower concentration of reactants in the zeolite pores (gas phase

vs liquid phase) and the shorter total time on stream, which is backed up by the silanol groups of the zeolite still being visible in the spectrum of the gas-phase alkylation sample. A similar behavior was observed by Kiricsi et al. [13]. Adsorption of pure butene on La-BEA immediately led to the formation of alkenyl ions, while upon adsorption of a 1-butene/isobutane mixture the formation of alkenyl ions was strongly suppressed. The decelerating effect of isobutane on the deactivation mechanism is twofold: (1) a high concentration of isobutane (achieved by high P/O ratios in the feed stream and by backmixing the reactor contents) slows down the buildup of high-molecular-weight compounds, which are the precursors of the alkenyl ions. (2) Isobutane competes in the hydride transfer step with the unsaturated compounds. A higher isobutane concentration will therefore inhibit the formation of enylic cations.

In liquid acids [25] and zeolites [43] at room temperature or below, alkenyl ions are the end product of such carbenium ion reactions. The situation changes at already moderately increased temperatures, as can be seen by the presence of aromatics in the deposits. A further deprotonation/hydride transfer step of a cyclohexenyl cation leads to a benzenium ion. The proton affinity of cyclohexadiene (837 kJ/mol) is significantly higher than the proton affinity of benzene (750 kJ/mol). Thus, a relatively high energy barrier must be overcome to form the benzenium ion. This should lead to a high-temperature sensitivity for the formation of these ions. A steep increase in aromatic protons with reaction temperature as measured with ^{1}H NMR confirms this hypothesis (see Fig. 10). At low reaction temperatures, most ions are of an aliphatic and naphtenic nature. Once the temperature is high enough, they are converted to aromatics. At even higher temperatures, polyaromatic compounds would be produced. The same trend is observed during the temperature-programmed desorption of the adsorbed deposits (see Fig. 4). Aromatics leave the zeolite pores only at temperatures above 200 °C, condensed aromatics above 300 °C. The desorption of aliphatic compounds has ceased completely at these temperatures. Since the deposit contains only a small amount of aromatics, most of the desorbing products must be produced in situ during the heating process. Performing the alkylation reaction at such high temperatures would give similar deposits as produced during the TPD [4]. It must be emphasized here that the difference in the nature of the deposits at low and high reaction temperatures is not reflected in the product distribution. Alkylation products leaving the zeolite pores at low temperatures are the same as at high temperatures, although they exhibit considerably different selectivities. This is concluded from the product chromatograms exhibiting the same peaks in all runs. Alkylation at 130 °C produces the same compounds as alkylation at 40 °C, although the deposits are significantly different.

The results presented in this study establish that only a fraction of the adsorbed species resembles the conjunct polymers formed in liquid acid-catalyzed alkylation. On the one hand, they contain alkanes and mono-olefins; on the other hand, they contain aromatic fragments. Both are not found within the conjunct polymers. While the former are alkylation and oligomerization products, the appearance of the latter is a consequence of the substantially higher reaction temperature with zeolites.

4.3. Interaction of the coke molecules with the acid sites

The question remains how the catalysts deactivate. In principle, two mechanisms are possible. These are pore blocking and site blocking/poisoning. The first mechanism implies that bulky molecules of arbitrary chemical nature grow in the catalyst pores. When these molecules reach a certain critical size, they cannot diffuse out and block the pores by *physical* presence. The second mechanism requires the formation of a strong *chemical* bond between the adsorbate and the active site. To discriminate between the two mechanisms, the deactivated catalysts are analyzed by nitrogen and pyridine adsorption (see Figs. 5 and 6). The minute concentration of mesopores shows that under these conditions the pores are completely full. Nitrogen as a nonpolar and nonbasic molecule cannot enter the micropore system at all (at the rather low temperature of 77 K, at which the adsorbed molecules are very rigid). Pyridine as a strong base, on the other hand, can enter and even replace some adsorbed species, as seen in the formation of the pyridinium ion and the negative hydrocarbon bands. A similar replacement has been described for zeolites coked in *m*-xylene transformation. Pyridine was found to replace a substantial amount of coke molecules. The authors observed a concomitant decrease of hydrocarbon bands upon adsorption of pyridine. Bands at 1350, 1505, 1590, and 1600 cm^{-1} wavenumbers were found to decrease or disappear [44]. The theoretical description of this phenomenon was given by Song et al., who studied the 1,3-dimethylcyclopentenyl carbenium ion ($C_7H_{11}^+$) adsorbed on H-ZSM-5. Coadsorption of basic molecules led to a deprotonation of the carbenium ion to form the neutral diene only when the employed base exhibited a proton affinity higher than the deprotonation enthalpy of the ion [45]. Only those reactions will be thermodynamically favored, which produce more stable carbenium ions. Pyridine with its very high proton affinity of 930 kJ/mol can replace almost all carbenium ions. Hydride transfer from the most abundant hydride transfer agent isobutane (having a proton affinity of 678 kJ/mol) to a substituted cyclopentenyl ion (a corresponding parent, e.g., 1-methylcyclopentene having a proton affinity of 817 kJ/mol) to give a simple isobutyl ion (or alkoxide) should therefore be highly unfavorable. Thus, once an acid site is occupied by a cycloalkenyl ion, it is lost for the alkylation chemistry. The steep increase in the MALDI signal intensity at the end of the active catalyst lifetime shown in Fig. 13 can be interpreted in line with this reasoning: When a significant number of acid sites is deactivated by alkenyl ions the remaining sites experience a higher butene concentration, which speeds up the formation of further alkenyl ions. The deactivation therefore is autoac-

celerated. This phenomenon is responsible for the sudden drop in conversion, which is often observed with solid acid alkylation catalysts.

H-BEA exhibited a similar behavior during pyridine and nitrogen adsorption. This material follows the same deactivation route as faujasitic catalysts. Differences arising from a different pore topology may be reflected in the lower CH_3/CH_2 ratio seen in the IR spectra of the deactivated catalysts, as shown in Fig. 2. The straight channels in zeolite BEA may not allow the same degree of branching that is possible in the more spacious supercages of faujasites.

Table 2 shows that the lifetime of La-H-X runs through a maximum at 75 °C. At both low and high reaction temperatures the lifetime is significantly lower. Assuming the irreversible adsorption of alkenyl ions to be the only deactivating route, the lifetime should be highest at low temperatures and constantly decline with increasing temperature, because of the increasingly unsaturated nature of the deposits. To account for the short lifetimes at low reaction temperatures, we attribute this to the strongly hindered diffusion of bulky high-molecular-weight alkanes. With increasing temperature, diffusion will be facilitated, but the increasing hydrogen deficiency of the molecules will bind them to the acid sites. Thus, the lifetime exhibits a maximum, at which the diffusion is sufficiently fast and the rate of formation of unsaturated compounds is still slow.

Deactivated faujasitic alkylation catalysts typically contain 10–20 wt% hydrocarbon deposits [4,8,46]. Assuming an average density for the deposits of 0.9 g/ml and a pore volume of 0.16 ml/g (see Table 1), roughly 15 wt% coke would fit in the pore system. This suggests that the pores of deactivated catalysts are completely filled. On the other hand, taking an acid site density of 0.6 mmol/g and an average molar mass of 250 g/mol for the molecules adsorbed on the acid sites also gives a coke loading of ca. 15 wt%. It can be concluded from this that almost all hydrocarbons in the zeolite pores are adsorbed on the acid sites, but at the end of the catalyst lifetime they completely fill the pore system. Since a substantial fraction of these compounds can be replaced by pyridine, some of them obviously are not too bulky to leave the pores. However, their chemical interaction with the acid sites strongly retains them in the pores. These calculations also rule out the assumption that carbonaceous species might preferentially grow on the outside and simply block the entrance into the pore system.

5. Conclusions

During zeolite-catalyzed isobutane/butene alkylation, which almost exclusively produces isoalkane products, a highly unsaturated and highly branched polymer is formed. The polymer is strongly adsorbed on the acid sites and completely fills the pores at the end of the reaction. With increasing reaction temperature, the deposits are increasingly hydrogen deficient and are of increasingly aromatic nature. The deposits contain compounds, which are similar to the conjunct polymers formed during alkylation with liquid acids. Additionally, zeolitic deposits contain alkanes and aromatics, which are not present in conjunct polymers.

MALDI-TOF MS and LDI-TOF MS both gave spectra when applied on the deactivated catalysts. MALDI most likely selectively detected oxidized products. Ions absorbing in the wavelength region of the laser were detected in the LDI experiments. Some of the aromatic molecules present in the deposits might have acted as matrices for other compounds. The molecular weight distribution is in good agreement with the distribution measured by GC-MS. However, the assignment of individual masses to certain types of compounds is still ambiguous. The interpretation of MALDI and LDI spectra should be of lesser complexity when used on catalysts with purely aromatic coke.

Acknowledgments

The authors thank Süd-Chemie AG for providing several of the examined samples. Financial support from Süd-Chemie AG is gratefully acknowledged. Dr. H.J. Räder from the Max-Planck-Institut für Polymerforschung, Mainz, is thanked for helpful discussions.

References

[1] A. Corma, A. Martinez, Catal. Rev.-Sci. Eng. 35 (1993) 483.
[2] J. Weitkamp, Y. Traa, in: G. Ertl, H. Knözinger, J. Weitkamp (Eds.), Handbook of Heterogeneous Catalysis, Vol. 4, VCH, Weinheim, 1997, p. 2039.
[3] E.H. van Broekhoven, F.R. Mas Cabre, P. Bogaard, G. Klaver, M. Vonhof, US patent 5,986,158, 1999.
[4] J. Weitkamp, S. Maixner, Zeolites 7 (1987) 6.
[5] M. Stöcker, H. Mostad, T. Rørvik, Catal. Lett. 28 (1994) 203.
[6] C. Flego, I. Kiricsi, W.O. Parker Jr., M.G. Clerici, Appl. Catal. A 124 (1995) 107.
[7] A.K. Nowak, C.M.A.M. Mesters, A.M. Rigby, D. Schulze, Preprints, Div. Petr. Chem., Am. Chem. Soc. 41 (1996) 668.
[8] J. Pater, F. Cardona, C. Canaff, N.S. Gnep, G. Szabo, M. Guisnet, Ind. Eng. Chem. Res. 38 (1999) 3822.
[9] R. Schöllner, H. Hölzel, Z. Chem. 15 (1975) 469.
[10] K. Yoo, E.C. Burckle, P.G. Smirniotis, Catal. Lett. 74 (2001) 85.
[11] F.A. Diaz-Mendoza, L. Pernett-Bolano, N. Cardona-Martinez, Thermochim. Acta 312 (1998) 47.
[12] G.S. Nivarthy, Y. He, K. Seshan, J.A. Lercher, J. Catal. 176 (1998) 192.
[13] I. Kiricsi, C. Flego, G. Bellussi, Appl. Catal. A 126 (1995) 401.
[14] M. Guisnet, P. Magnoux, Appl. Catal. A 212 (2001) 83.
[15] S.D. Hanton, Chem. Rev. 101 (2001) 527.
[16] M.C. Fitzgerald, G. Siuzdak, Chem. Biol. 3 (1996) 707.
[17] M. Yang, J.P. Reilly, J. Phys. Chem. 94 (1990) 6299.
[18] R. Zenobi, R. Knochenmuss, Mass Spectrom. Rev. 17 (1998) 337.
[19] G. Kühn, S. Weidner, U. Just, G. Hohner, J. Chromatogr. A 732 (1996) 111.
[20] T.K. Dutta, S. Harayama, Anal. Chem. 73 (2001) 864.
[21] J.K. Pruns, J.P. Vietzke, M. Strassner, C. Rapp, U. Hintze, W.A. König, Rapid Commun. Mass Spectrom. 16 (2002) 208.
[22] R.B. Borade, A. Clearfield, J. Phys. Chem. 96 (1992) 6729.

[23] A. Feller, A. Guzman, I. Zuazo, J.A. Lercher, (2003), submitted for publication.
[24] J.C. Evans, in: G.A. Olah, P.R. Schleyer (Eds.), Carbonium Ions, Vol. 1, Interscience, New York, 1968, p. 223.
[25] N.C. Deno, in: G.A. Olah, P.R. Schleyer (Eds.), Carbonium Ions, Vol. 2, Interscience, New York, 1970, p. 783.
[26] I. Kiricsi, H. Förster, J. Chem. Soc., Faraday Trans. 84 (1988) 491.
[27] I. Kiricsi, H. Förster, G. Tasi, J.B. Nagy, Chem. Rev. 99 (1999) 2085.
[28] D. Eisenbach, E. Gallei, J. Catal. 56 (1979) 377.
[29] A.W. Ehlers, C.G. de Koster, R.J. Meier, K. Lammertsma, J. Phys. Chem. A 105 (2001) 8691.
[30] R. Knochenmuss, F. Dubois, M.J. Dale, R. Zenobi, Rapid Commun. Mass Spectrom. 10 (1996) 871.
[31] N.C. Deno, J. Bollinger, N. Friedman, K. Hafer, J.D. Hodge, J.J. Houser, J. Am. Chem. Soc. 85 (1963) 2998.
[32] G.A. Olah, C.U. Pittman, M.C.R. Symons, in: G.A. Olah, P.R. Schleyer (Eds.), Carbonium Ions, Vol. 1, Interscience, New York, 1968, p. 153.
[33] S.F. Macha, T.D. McCarley, P.A. Limbach, Anal. Chim. Acta 397 (1999) 235.
[34] T. Kinumi, T. Saisu, M. Takayama, H. Niwa, J. Mass Spectrom. 35 (2000) 417.
[35] L.F. Albright, Chemtech June (1998) 40.
[36] L.F. Albright, M.A. Spalding, C.G. Kopser, R.E. Eckert, Ind. Eng. Chem. Res. 27 (1988) 386.
[37] L. Miron, R.J. Lee, J. Chem. Eng. Data 8 (1963) 150.
[38] T.S. Sorensen, in: G.A. Olah, P.R. Schleyer (Eds.), Carbonium Ions, Vol. 2, Interscience, New York, 1970, p. 807.
[39] J.B. Nicholas, J.F. Haw, J. Am. Chem. Soc. 120 (1998) 11804.
[40] S. Yang, J.N. Kondo, K. Domen, Catal. Today 73 (2002) 113.
[41] N.C. Deno, D.B. Boyd, J.D. Hodge, C.U. Pittman, J.O. Turner, J. Am. Chem. Soc. 86 (1964) 1745.
[42] G.A. Olah, J.A. Olah, in: G.A. Olah, P.R. Schleyer (Eds.), Carbonium Ions, Vol. 2, Interscience, New York, 1970, p. 715.
[43] H. Förster, I. Kiricsi, Zeolites 7 (1987) 508.
[44] H.S. Cerqueira, P. Ayrault, J. Datka, M. Guisnet, Micropor. Mesopor. Mater. 38 (2000) 197.
[45] W. Song, J.B. Nicholas, J.F. Haw, J. Am. Chem. Soc. 123 (2001) 121.
[46] C.A. Querini, Catal. Today 62 (2000) 135.